Science Advances
AAAS

Supplementary Materials for

A computational mechanism of cue-stimulus integration for pain in the brain

Jungwoo Kim *et al.*

Corresponding author: Seng Bum Michael Yoo, sbyoo@g.skku.edu; Choong-Wan Woo, waniwoo@skku.edu

Sci. Adv. **10**, eado8230 (2024)
DOI: 10.1126/sciadv.ado8230

This PDF file includes:

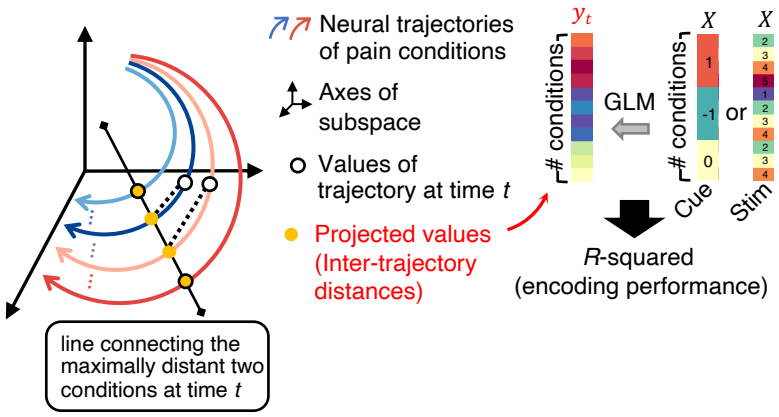

Fig. S1. Calculating encoding performances. Calculating encoding performance. Group average FIR time-series data projected onto cue and stimulus subspaces create neural trajectories, represented by colored lines. We selected the two most distant conditions among trajectories at single time points (yellow dots with black outlines) and then drew the line that connects the two. We then projected the same time point (white dots with black outlines) of other trajectories onto the line, resulting in a one-dimensional vector (yellow dots) that encoded distance information between trajectories. This is what we referred to as inter-trajectory distances, which we used to calculate encoding performances and reconstruct pain ratings.

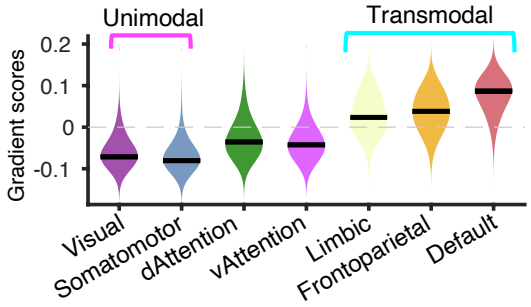

Fig. S2. Principal gradient scores from the resting-state fMRI data of the participants in this study. The figure shows voxel-wise principal gradient scores from the first gradient of the whole-brain resting-state fMRI ($N = 56$). We used diffusion embedding implemented in the BrainSpace Toolbox (*99*) for the calculation of the gradient. The gradient scores for each network were obtained using the network mask employed in the current study. Resting-state data were up-sampled to 3 mm for the gradient calculation.

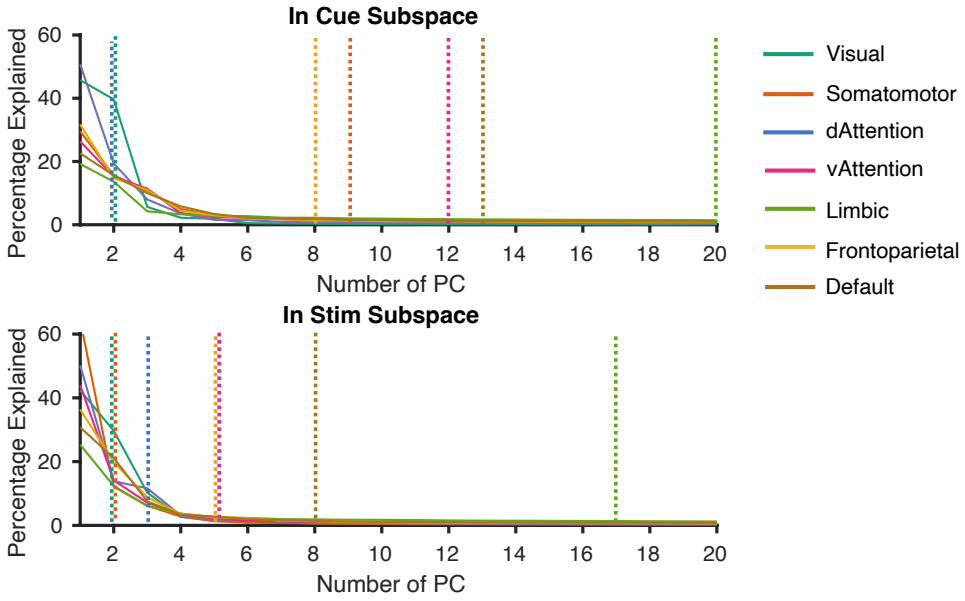

Fig. S3. The variance explained by the principal components constituting the cue and stimulus subspaces. The upper panel displays the variance explained by principal components constituting the cue subspace, while the lower panel displays the variance explained by principal components constituting the stimulus subspace. Dashed lines represent the number of principal components explaining 70% variance for each network. We used 20 dimensions for all networks to control for differences arising from the different number of dimensions. With 20 dimensions, the percentage of explained variance in the cue subspace ranges from 70% in the limbic network to 97% in the visual network. In the stimulus subspace, it ranges from 74% in the limbic network to 94% in the visual network.

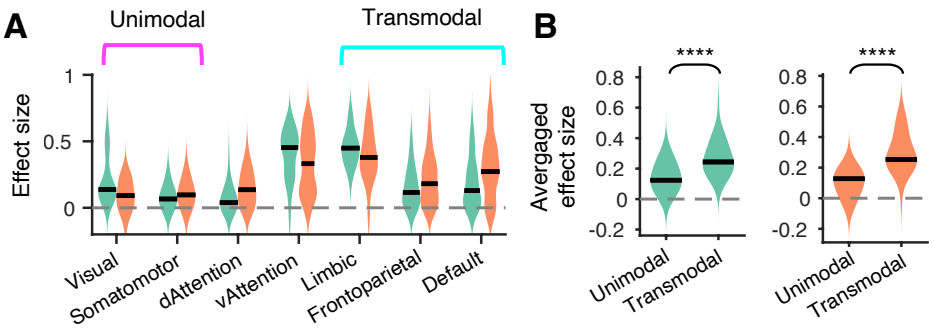

Fig. S4. Effect sizes of large-scale networks. (A) Effect sizes, calculated as the subtraction of null encoding performances from the actual encoding performances, for all seven networks. The green plots show effect sizes in the cue subspace, and the orange plots show effect sizes of the stimulus subspace. **(B)** Averages of cue and stimulus effect sizes across networks. The left panel displays the effect sizes for the cue subspace, while the right panel illustrates the effect sizes of the stimulus subspace. $^{****}p < 0.0001$, two-tailed, paired *t*-test.

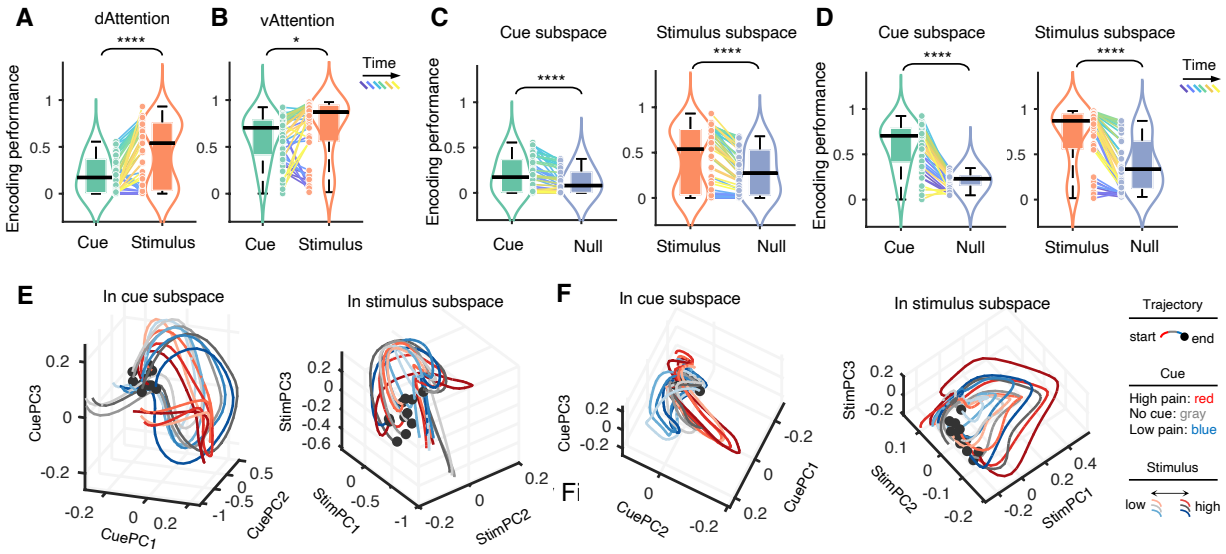

Fig. S5. Encoding performances and neural trajectories of the dorsal attention (dAttention) and ventral attention (vAttention) networks. (A-B) Encoding performances of the dAttention **(A)** and vAttention networks **(B)**. The encoding performances of the stimulus were significantly larger than those of the cue in both dAttention network (t_{48} = 5.626, p = 9.286 e-7, two-tailed, paired t-test) and vAttention network (t_{48} = 2.628, p = 0.012, two-tailed, paired t-test). The layout is the same as Figs. 4A-C, D**.** The encoding performances were based on the actual versus null subspaces of the dAttention **(C)** and vAttention networks **(D)**. **(E-F)** Neural trajectories of the dAttention **(E)** and vAttention networks **(F)**. The trajectories were smoothed with a Gaussian kernel (standard deviation: 3 TRs) for visualization purposes, but the unsmoothed trajectories were employed for the actual analysis. The layout is the same as **Figs. 4G-I**. * $p < 0.05$; **** $p <$ 0.0001, two-tailed, paired t-test.

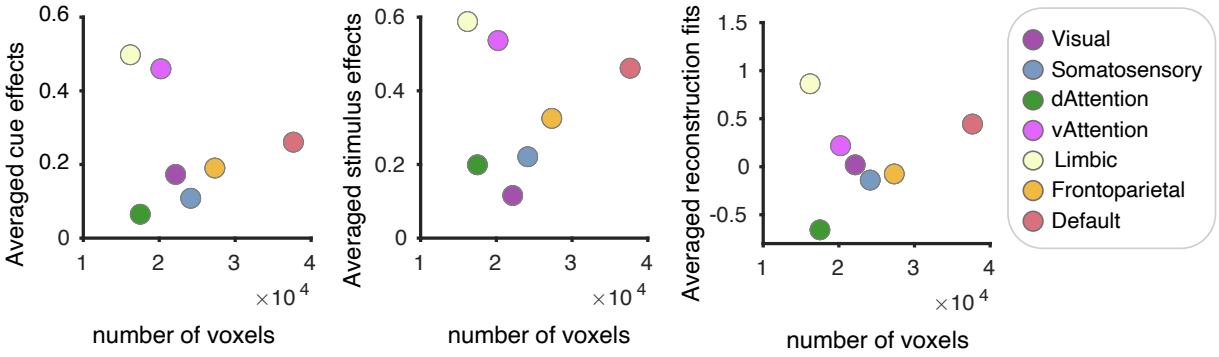

Fig. S6. Relationship between effect sizes and the network sizes. Network-level statistics—cue effects, stimulus effects, and reconstruction fits—were compared with their number of voxels within each network. We calculated Spearman's rank correlation between the temporal averages of these statistics and the number of voxels for each network to account for their different scales. From the left panel to the right panel, each panel shows the number of voxels on the x-axis and cue effects, stimulus effects, and reconstruction fits on the y-axis, respectively, all of which showed no significant correlation. (cue effects: r_s = -0.143, p = 0.783; stimulus effects: r_s = -0.179, p = 0.713; reconstruction fits: r_s = -0.071, p = 0.906; two-tailed, Spearman's rank correlation)

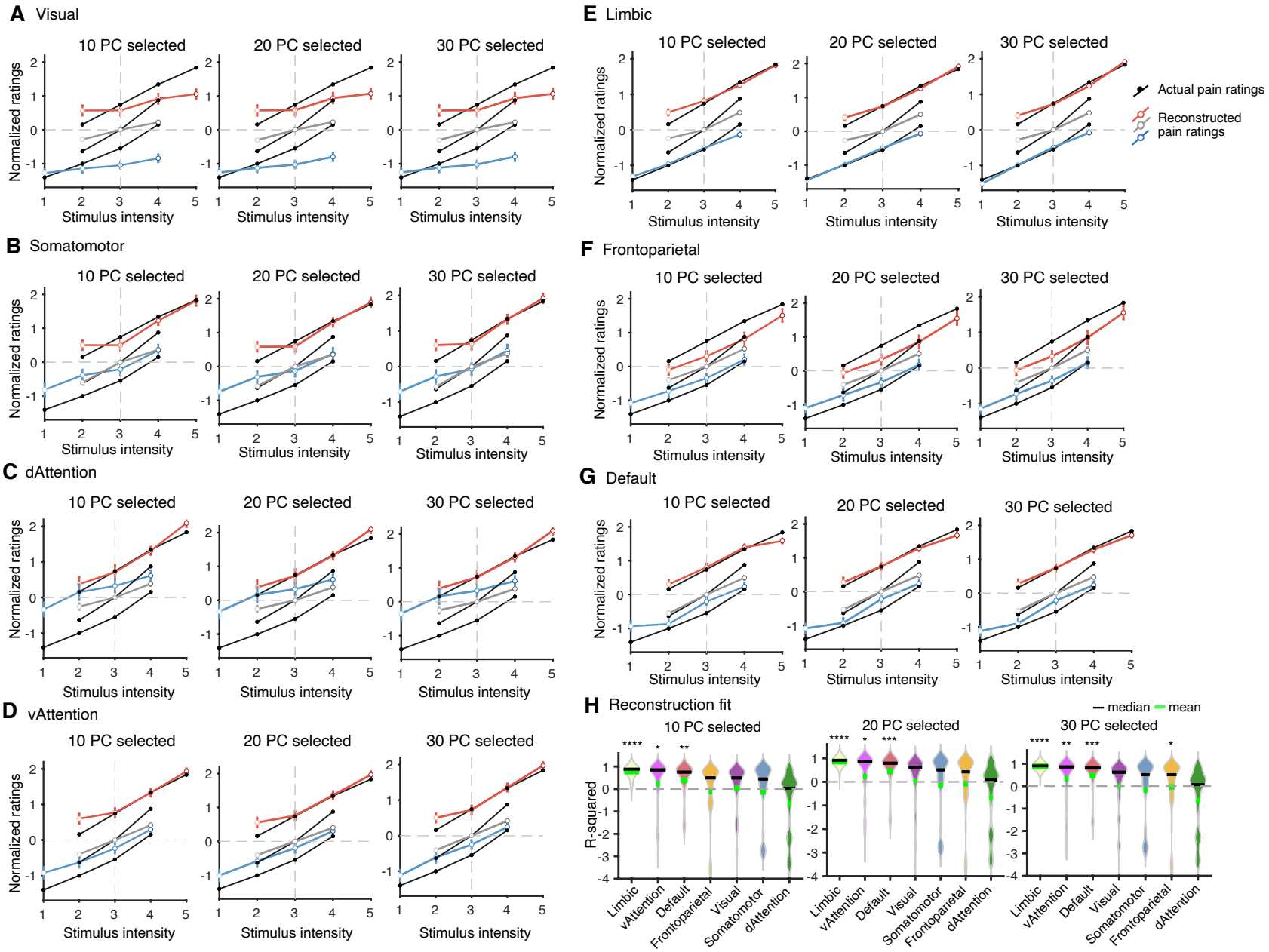
A Visual
10 PC selected
20 PC selected
30 PC selected
Normalized ratings
Stimulus intensity
B Somatomotor
C dAttention
D vAttention
E Limbic
F Frontoparietal
G Default
Actual pain ratings
Reconstructed pain ratings
H Reconstruction fit
median
mean
R-squared
Limbic
vAttention
Default
Frontoparietal
Visual
Somatomotor
dAttention

Fig. S7. Reconstructed pain ratings using a different number of principal components (PCs). (A-G) Comparison of the actual and reconstructed pain ratings from each of the 7 large-scale networks. In all figures, the left panel shows reconstructed pain ratings from neural trajectories within cue and stimulus subspaces of 10 PCs. The middle and the right panels show the results using 20 PCs and 30 PCs, respectively. The colored (red, blue, and gray) lines indicate the reconstructed pain ratings, while the black lines indicate average pain ratings across participants. Both metrics are normalized for comparison between the two. **(H)** Reconstruction fits from each network using a different number of PCs. These were calculated as *R*-squared values of the reconstructed ratings for every time point. Results obtained using 20 PCs are also included in the main figures and results. In all cases, reconstruction fits were significant for the limbic, default mode, and vAttention networks. In the limbic network, using 10 PCs, md (median) = 0.883, $z = 6.088$, $p = 5.236$ e-10; 30 PCs, md = 0.905, $z = 6.088$, $p = 5.236$ e-10. In the default network, using 10 PCs, md = 0.752, $z = 2.944$, $p = 0.002$; 30 PCs, md = 0.806, $z = 3.342$, $p = 4$ e-4. In the vAttention network, using 10 PCs, md = 0.852, $z = 2.139$, $p = 0.016$; 30 PCs, md = 0.856, $z = 2.586$, $p = 0.005$. Note that using 30 PCs showed significant reconstruction fit also in the frontoparietal network (md = 0.506, $z = 1.870$, $p = 0.031$). All p values are one-tailed and from Wilcoxon signed rank test with 49 time points. Networks are aligned in a descending order of the median. The results with 20 PCs are presented as the main results and figures. $^{*}p < 0.05$, $^{**}p < 0.01$, $^{***}p < 0.001$, $^{****}p < 0.0001$.

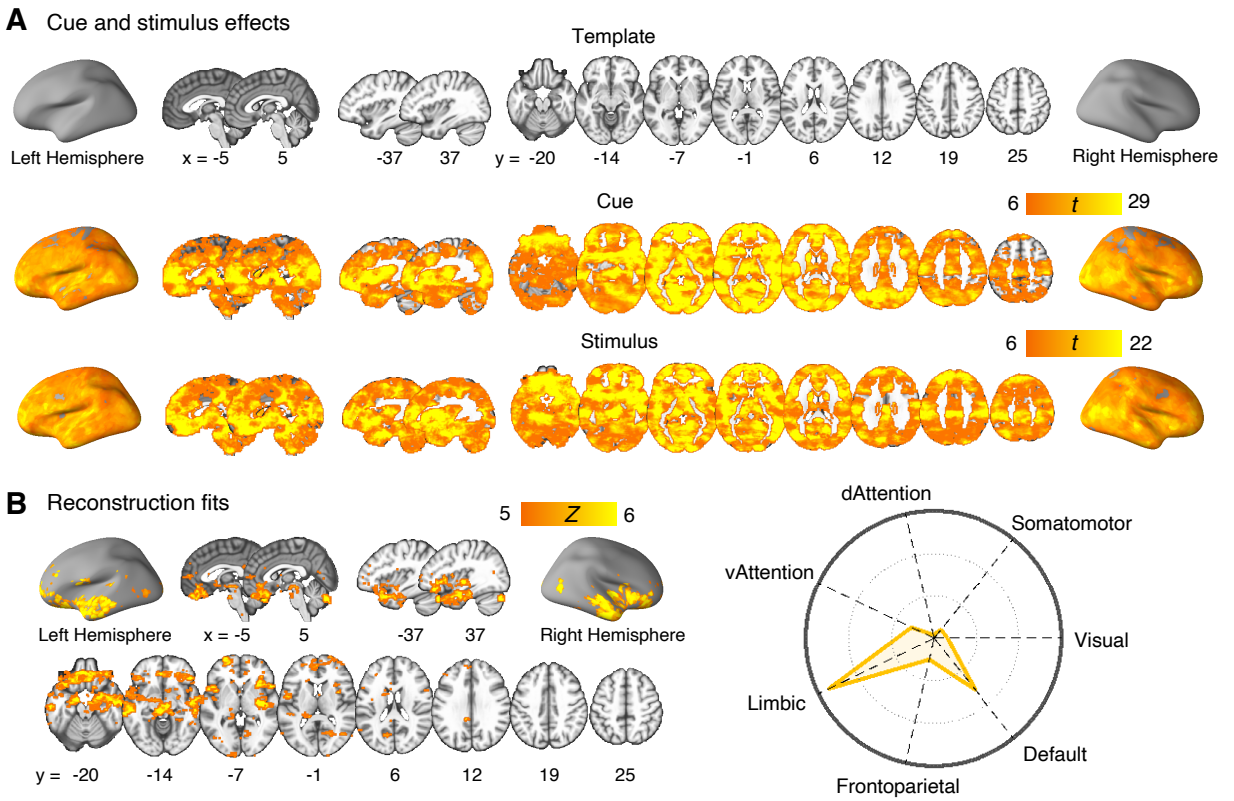

Fig. S8. Results of searchlight analysis. We conducted searchlight analyses for all gray matter voxels. The spherical searchlight radius size was 5 voxels. **(A)** Voxels with significant cue (middle panel) and stimulus (lower panel) encoding performances. Significance was determined using a paired *t*-test, with $df = 48$, Bonferroni corrected $p < 0.05$. The upper panel displays the template brain, with each column corresponding to the same spatial axis as in the middle and lower panels. **(B)** Voxels with significant reconstruction fit (left panel) and the radial plot showing proportions of significant voxels within a large-scale network (right panel). Significance follows the same criterion as in **(A)**, but with a one-tailed Wilcoxon signed rank test. In the radial plot, the proportions occupied by each network were calculated as the number of occupying voxels divided by the total voxel count of the respective network.

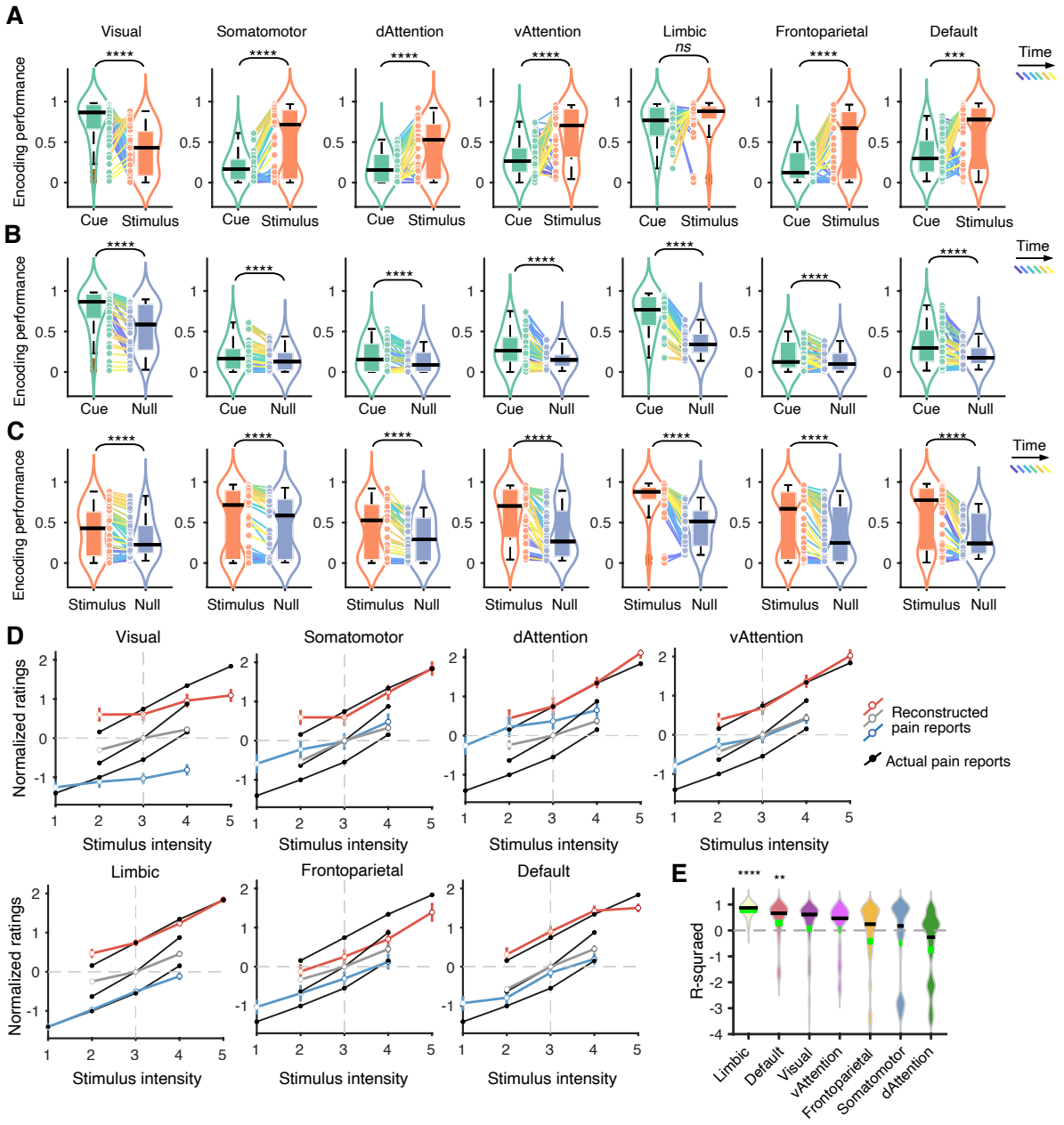

Fig. S9. Encoding performances and reconstruction fits of large-scale networks comprising only the cerebrum. **(A)** Encoding performances of all 7 large-scale networks. The encoding performance was calculated for each time point, and the plots show the time information with the graded colors ranging from cool (early) to warm (late) colors. **(B)** Encoding performances based on the actual cue subspace versus the null subspace. **(C)** Encoding performances based on the actual stimulus subspace versus the null subspace. **(D)** The colored (red, blue, and gray) lines show the reconstructed pain ratings from distances of neural trajectories in subspaces, and black lines indicate averaged pain ratings from participants, also normalized for comparisons with the reconstructed pain ratings. The error bars indicate SEM across time. **(E)** Reconstruction fits of the large-scale networks. Reconstruction fits were calculated with *R*-squared values of the reconstructed pain rating at each time point. Networks are aligned in a descending order of the median. $^{*}p < 0.05$, $^{**}p < 0.01$, $^{***}p < 0.001$, $^{****}p < 0.0001$

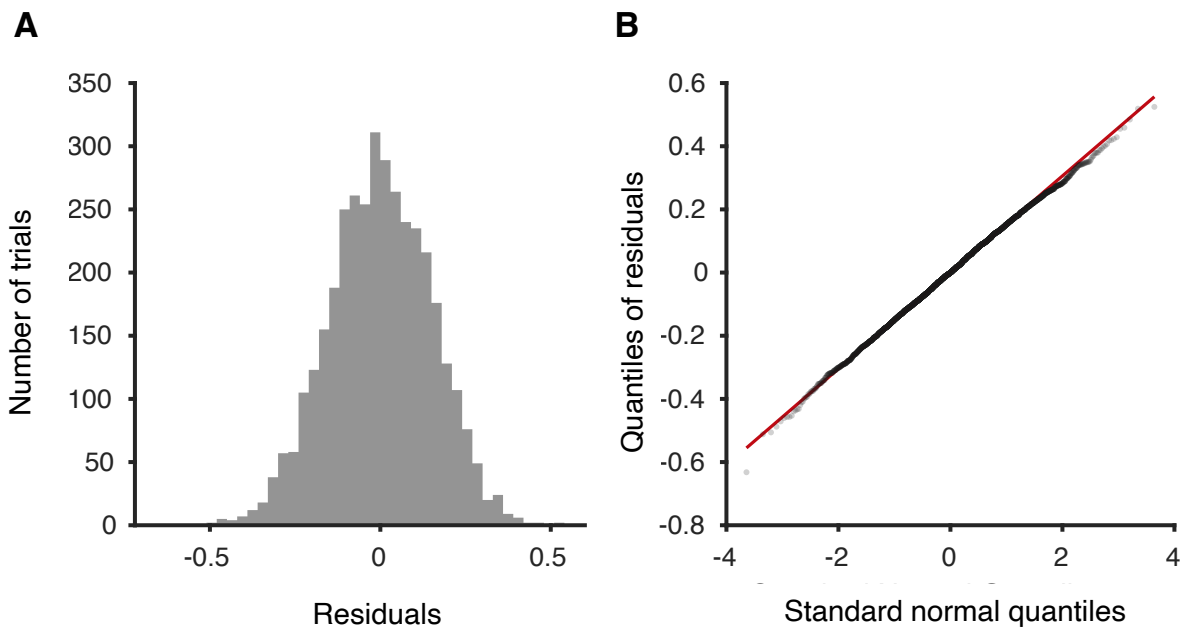

Fig. S10. Residuals from multilevel GLM of behavioral data. (A) A histogram of trial-level residuals of pain ratings after accounting for the effects of cues, stimulus intensities, their interactions, and participants. **(B)** A Quantile-Quantile plot of the residuals of pain ratings. The dots indicate the residuals of single trials, and the red line represents the expected distribution if the residuals perfectly follow a normal distribution.

Table S1. Effect sizes with different numbers of principal components

Networks	Cue						Stimulus					
	NumPC 10		NumPC 20		NumPC 30		NumPC 10		NumPC 20		NumPC 30	
	t	*p*	*t*	*p*	*t*	*p*	*t*	*p*	*t*	*p*	*t*	*p*
Visual	8.932	8.932E-12	8.243	9.466E-11	8.107	1.517E-10	5.604	1.002E-06	5.818	4.753E-07	5.919	3.333E-07
Somatosensory	7.473	1.388E-09	7.366	2.021E-09	7.547	1.071E-09	7.533	1.125E-09	7.451	1.502E-09	7.889	3.247E-10
dAttention	5.364	2.310E-06	5.142	4.962E-06	5.098	5.772E-06	8.043	1.899E-10	7.977	2.388E-10	7.944	2.678E-10
vAttention	14.979	1.013E-19	14.482	3.830E-19	15.211	5.487E-20	8.279	8.364E-11	10.211	1.273E-13	11.632	1.431E-15
Limbic	16.630	1.484E-21	24.801	5.089E-29	30.604	3.810E-33	9.546	1.132E-12	13.718	3.148E-18	18.528	1.646E-23
Frontoparietal	6.551	3.598E-08	7.322	2.362E-09	7.963	2.503E-10	8.483	4.136E-11	8.220	1.026E-10	8.510	3.780E-11
Default	6.589	3.144E-08	7.126	4.717E-09	8.192	1.130E-10	7.663	7.145E-10	9.135	4.495E-12	9.826	4.483E-13

Note. The table shows *t*-values and *p* values of cue and stimulus effect sizes from paired *t*-test (*df* = 48, two-tailed). We calculated cue and stimulus effect sizes in all 7 large-scale networks using different numbers of principal components (denoted as NumPC). The results remained significant regardless of the number of PCs constituting the subspaces. Results obtained using the 20 PCs are presented as the main results and figures.

REFERENCES

1. A. I. Basbaum, D. M. Bautista, G. Scherrer, D. Julius, Cellular and molecular mechanisms of pain. *Cell* **139**, 267–284 (2009).

2. L. Y. Atlas, T. D. Wager, How expectations shape pain. *Neurosci. Lett.*, **520**, 140–148 (2012).

3. H. L. Fields, How expectations influence pain. *Pain* **159**, S3–S10 (2018).

4. B. Seymour, F. Mancini, Hierarchical models of pain: Inference, information-seeking, and adaptive control. *Neuroimage* **222**, 117212 (2020).

5. K. Wiech, Deconstructing the sensation of pain: The influence of cognitive processes on pain perception. *Science* **354**, 584–587 (2016).

6. N. Fallon, C. Roberts, A. Stancak, Shared and distinct functional networks for empathy and pain processing: A systematic review and meta-analysis of fMRI studies. *Soc. Cogn. Affect. Neurosci.* **15**, 709–723 (2020).

7. V. A. Apkarian, J. A. Hashmi, M. N. Baliki, Pain and the brain: Specificity and plasticity of the brain in clinical chronic pain. *Pain* **152**, S49–S64 (2011).

8. A. Watson, W. El-Deredy, G. D. Iannetti, D. Lloyd, I. Tracey, B. A. Vogt, V. Nadeau, A. K. P. Jones, Placebo conditioning and placebo analgesia modulate a common brain network during pain anticipation and perception. *Pain* **145**, 24–30 (2009).

9. K. Wiech, M. Ploner, I. Tracey, Neurocognitive aspects of pain perception. *Trends Cogn. Sci.* **12**, 306–313 (2008).

10. C.-W. Woo, M. Roy, J. T. Buhle, T. D. Wager, Distinct brain systems mediate the effects of nociceptive input and self-regulation on pain. *PLoS Biol.* **13**, e1002036 (2015).

11. R. C. Coghill, C. N. Sang, J. M. Maisog, M. J. Iadarola, Pain intensity processing within the human brain: A bilateral, distributed mechanism. *J. Neurophysiol.* **82**, 1934–1943 (1999).

12. C. J. Vierck, B. L. Whitsel, O. V. Favorov, A. W. Brown, M. Tommerdahl, Role of primary somatosensory cortex in the coding of pain. *Pain* **154**, 334–344 (2013).

13. P. Rainville, G. H. Duncan, D. D. Price, B. Carrier, M. C. Bushnell, Pain affect encoded in human anterior cingulate but not somatosensory cortex. *Science* **277**, 968–971 (1997).

14. S. Vyas, M. D. Golub, D. Sussillo, K. V. Shenoy, Computation through neural population dynamics. *Annu. Rev. Neurosci.* **43**, 249–275 (2020).

15. C. J. MacDowell, T. J. Buschman, Low-dimensional spatiotemporal dynamics underlie cortex-wide neural activity. *Curr. Biol.* **30**, 2665–2680.e8 (2020).

16. S. Saxena, J. P. Cunningham, Towards the neural population doctrine. *Curr. Opin. Neurobiol.* **55**, 103–111 (2019).

17. R. B. Ebitz, B. Y. Hayden, The population doctrine in cognitive neuroscience. *Neuron* **109**, 3055–3068 (2021).

18. A. Nair, T. Karigo, B. Yang, S. Ganguli, M. J. Schnitzer, S. W. Linderman, D. J. Anderson, A. Kennedy, An approximate line attractor in the hypothalamus encodes an aggressive state. *Cell* **186**, 178–193.e15 (2023).

19. H. Sohn, D. Narain, N. Meirhaeghe, M. Jazayeri, Bayesian computation through cortical latent dynamics. *Neuron* **103**, 934–947.e5 (2019).

20. C. Langdon, M. Genkin, T. A. Engel, A unifying perspective on neural manifolds and circuits for cognition. *Nat. Rev. Neurosci.* **24**, 363–377 (2023).

21. L. M. Boyle, L. Posani, S. Irfan, S. A. Siegelbaum, S. Fusi, Tuned geometries of hippocampal representations meet the computational demands of social memory. *Neuron* **112,** 1358–1371.e9 (2024).

22. Y. Xie, P. Hu, J. Li, J. Chen, W. Song, X.-J. Wang, T. Yang, S. Dehaene, S. Tang, B. Min, L. Wang, Geometry of sequence working memory in macaque prefrontal cortex. *Science* **375**, 632–639 (2022).

23. D. S. Margulies, S. S. Ghosh, A. Goulas, M. Falkiewicz, J. M. Huntenburg, G. Langs, G. Bezgin, S. B. Eickhoff, F. X. Castellanos, M. Petrides, E. Jefferies, J. Smallwood, Situating the default-mode network along a principal gradient of macroscale cortical organization. *Proc. Natl. Acad. Sci. U.S.A.* **113**, 12574–12579 (2016).

24. U. Hasson, J. Chen, C. J. Honey, Hierarchical process memory: Memory as an integral component of information processing. *Trends Cogn. Sci.* **19**, 304–313 (2015).

25. J. M. Huntenburg, P.-L. Bazin, D. S. Margulies, Large-scale gradients in human cortical organization. *Trends Cogn. Sci.* **22**, 21–31 (2018).

26. V. Mante, D. Sussillo, K. V. Shenoy, W. T. Newsome, Context-dependent computation by recurrent dynamics in prefrontal cortex. *Nature* **503**, 78–84 (2013).

27. M. C. Aoi, V. Mante, J. W. Pillow, Prefrontal cortex exhibits multidimensional dynamic encoding during decision-making. *Nat. Neurosci.* **23**, 1410–1420 (2020).

28. B. T. T. Yeo, F. M. Krienen, J. Sepulcre, M. R. Sabuncu, D. Lashkari, M. Hollinshead, J. L. Roffman, J. W. Smoller, L. Zöllei, J. R. Polimeni, B. Fischl, H. Liu, R. L. Buckner, The organization of the human cerebral cortex estimated by intrinsic functional connectivity. *J. Neurophysiol.* **106**, 1125–1165 (2011).

29. E. Y. Choi, B. T. T. Yeo, R. L. Buckner, The organization of the human striatum estimated by intrinsic functional connectivity. *J. Neurophysiol.* **108**, 2242–2263 (2012).

30. R. L. Buckner, F. M. Krienen, A. Castellanos, J. C. Diaz, B. T. T. Yeo, The organization of the human cerebellum estimated by intrinsic functional connectivity. *J. Neurophysiol.* **106**, 2322–2345 (2011).

31. M. T. Kaufman, M. M. Churchland, S. I. Ryu, K. V. Shenoy, Cortical activity in the null space: Permitting preparation without movement. *Nat. Neurosci.* **17**, 440–448 (2014).

32. S. B. M. Yoo, B. Y. Hayden, The transition from evaluation to selection involves neural subspace reorganization in core reward regions. *Neuron* **105**, 712–724.e4 (2020).

33. I. Voitov, T. D. Mrsic-Flogel, Cortical feedback loops bind distributed representations of working memory. *Nature* **608**, 381–389 (2022).

34. C. Tang, R. Herikstad, A. Parthasarathy, C. Libedinsky, S.-C. Yen, Minimally dependent activity subspaces for working memory and motor preparation in the lateral prefrontal cortex. *eLife*, **9**, 58154 (2020).

35. Z. Fu, D. Beam, J. M. Chung, C. M. Reed, A. N. Mamelak, R. Adolphs, U. Rutishauser, The geometry of domain-general performance monitoring in the human medial frontal cortex. *Science* **376**, eabm9922 (2022).

36. G. Okazawa, C. E. Hatch, A. Mancoo, C. K. Machens, R. Kiani, Representational geometry of perceptual decisions in the monkey parietal cortex. *Cell* **184**, 3748–3761.e18 (2021).

37. S. Bernardi, M. K. Benna, M. Rigotti, J. Munuera, S. Fusi, C. D. Salzman, The geometry of abstraction in the hippocampus and prefrontal cortex. *Cell* **183**, 954–967.e21 (2020).

38. V. J. Sydnor, B. Larsen, D. S. Bassett, A. Alexander-Bloch, D. A. Fair, C. Liston, A. P. Mackey, M. P. Milham, A. Pines, D. R. Roalf, J. Seidlitz, T. Xu, A. Raznahan, T. D. Satterthwaite, Neurodevelopment of the association cortices: Patterns, mechanisms, and implications for psychopathology. *Neuron* **109**, 2820–2846 (2021).

39. R. V. Raut, A. Z. Snyder, M. E. Raichle, Hierarchical dynamics as a macroscopic organizing principle of the human brain. *Proc. Natl. Acad. Sci. U.S.A.* **117**, 20890–20897 (2020).

40. A. Samara, J. Eilbott, D. S. Margulies, T. Xu, T. Vanderwal, Cortical gradients during naturalistic processing are hierarchical and modality-specific. *Neuroimage* **271**, 120023 (2023).

41. Z. Huang, G. A. Mashour, A. G. Hudetz, Functional geometry of the cortex encodes dimensions of consciousness. *Nat. Commun.* **14**, 72 (2023).

42. T. Ito, J. D. Murray, Multitask representations in the human cortex transform along a sensory-to-motor hierarchy. *Nat. Neurosci.* **26**, 306–315 (2023).

43. R. V. Raut, A. Z. Snyder, A. Mitra, D. Yellin, N. Fujii, R. Malach, M. E. Raichle, Global waves synchronize the brain's functional systems with fluctuating arousal. *Sci. Adv.* **7**, eabf2709 (2021).

44. G. F. Elsayed, A. H. Lara, M. T. Kaufman, M. M. Churchland, J. P. Cunningham, Reorganization between preparatory and movement population responses in motor cortex. *Nat. Commun.* **7**, 13239 (2016).

45. M. D. Golub, P. T. Sadtler, E. R. Oby, K. M. Quick, S. I. Ryu, E. C. Tyler-Kabara, A. P. Batista, S. M. Chase, B. M. Yu, Learning by neural reassociation. *Nat. Neurosci.* **21**, 607–616 (2018).

46. J. Weber, G. Iwama, A.-K. Solbakk, A. O. Blenkmann, P. G. Larsson, J. Ivanovic, R. T. Knight, T. Endestad, R. Helfrich, Subspace partitioning in the human prefrontal cortex resolves cognitive interference. *Proc. Natl. Acad. Sci. U.S.A.* **120**, e2220523120 (2023).

47. A. Libby, T. J. Buschman, Rotational dynamics reduce interference between sensory and memory representations. *Nat. Neurosci.* **24**, 715–726 (2021).

48. A. C. Snyder, B. M. Yu, M. A. Smith, A stable population code for attention in prefrontal cortex leads a dynamic attention code in visual cortex. *J. Neurosci.* **41**, 9163–9176 (2021).

49. D. L. Kimmel, G. F. Elsayed, J. P. Cunningham, W. T. Newsome, Value and choice as separable and stable representations in orbitofrontal cortex. *Nat. Commun.* **11**, 3466 (2020).

50. J. A. Gallego, M. G. Perich, S. N. Naufel, C. Ethier, S. A. Solla, L. E. Miller, Cortical population activity within a preserved neural manifold underlies multiple motor behaviors. *Nat. Commun.* **9**, 4233 (2018).

51. M. M. Churchland, J. P. Cunningham, M. T. Kaufman, J. D. Foster, P. Nuyujukian, S. I. Ryu, K. V. Shenoy, K. V. Shenoy, Neural population dynamics during reaching. *Nature* **487**, 51–56 (2012).

52. D. Thura, J. F. Cabana, A. Feghaly, P. Cisek, Integrated neural dynamics of sensorimotor decisions and actions. *PLoS Biol.* **20**, e3001861 (2022).

53. E. L. Sylwestrak, Y. J. Jo, S. Vesuna, X. Wang, B. Holcomb, R. H. Tien, D. K. Kim, L. Fenno, C. Ramakrishnan, W. E. Allen, R. Chen, K. V. Shenoy, D. Sussillo, K. Deisseroth, Cell-type-specific population dynamics of diverse reward computations. *Cell* **185**, 3568–3587.e27 (2022).

54. M. Khona, I. R. Fiete, Attractor and integrator networks in the brain. *Nat. Rev. Neurosci.* **23**, 744–766 (2022).

55. D. Senkowski, M. Höfle, A. K. Engel, Crossmodal shaping of pain: A multisensory approach to nociception. *Trends Cogn. Sci.* **18**, 319–327 (2014).

56. N. Kriegeskorte, R. Cusack, P. Bandettini, How does an fMRI voxel sample the neuronal activity pattern: Compact-kernel or complex spatiotemporal filter?, *Neuroimage* **49**, 1965–1976 (2010).

57. L. Cocchi, A. Zalesky, A. Fornito, J. B. Mattingley, Dynamic cooperation and competition between brain systems during cognitive control. *Trends Cogn. Sci.* **17**, 493–501 (2013).

58. J. Kong, K. Jensen, R. Loiotile, A. Cheetham, H.-Y. Wey, Y. Tan, B. Rosen, J. W. Smoller, T. J. Kaptchuk, R. L. Gollub, Functional connectivity of the frontoparietal network predicts cognitive modulation of pain. *Pain* **154**, 459–467 (2013).

59. J. Lorenz, S. Minoshima, K. L. Casey, Keeping pain out of mind: The role of the dorsolateral prefrontal cortex in pain modulation. *Brain* **126**, 1079–1091 (2003).

60. D. A. Seminowicz, M. Moayedi, The dorsolateral prefrontal cortex in acute and chronic pain. *J. Pain* **18**, 1027–1035 (2017).

61. V. Legrain, S. Van Damme, C. Eccleston, K. D. Davis, D. A. Seminowicz, G. Crombez, A neurocognitive model of attention to pain: Behavioral and neuroimaging evidence. *Pain* **144**, 230–232 (2009).

62. D. A. Seminowicz, K. D. Davis, Interactions of pain intensity and cognitive load: The brain stays on task. *Cereb. Cortex* **17**, 1412–1422 (2007).

63. M. T. Wallace, R. Ramachandran, B. E. Stein, A revised view of sensory cortical parcellation. *Proc. Natl. Acad. Sci. U.S.A.* **101**, 2167–2172 (2004).

64. S. A. Koay, A. S. Charles, S. Y. Thiberge, C. D. Brody, D. W. Tank, Sequential and efficient neural-population coding of complex task information. *Neuron* **110**, 328–349.e11 (2022).

65. L. Pinto, K. Rajan, B. DePasquale, S. Y. Thiberge, D. W. Tank, C. D. Brody, Task-dependent changes in the large-scale dynamics and necessity of cortical regions. *Neuron* **104**, 810–824.e9 (2019).

66. T. T. Rogers, J. L. McClelland, Parallel distributed processing at 25: Further explorations in the microstructure of cognition. *Cognit. Sci.* **38**, 1024–1077 (2014).

67. S. B. M. Yoo, B. Y. Hayden, Economic choice as an untangling of options into actions. *Neuron* **99**, 434–447 (2018).

68. J. A. Fodor, *The Modularity of Mind* (MIT Press, 1983).

69. B. T. T. Yeo, F. M. Krienen, S. B. Eickhoff, S. N. Yaakub, P. T. Fox, R. L. Buckner, C. L. Asplund, M. W. L. Chee, Functional specialization and flexibility in human association cortex. *Cereb. Cortex* **25**, 3654–3672 (2015).

70. F. Mancini, S. Zhang, B. Seymour, Computational and neural mechanisms of statistical pain learning. *Nat. Commun.* **13**, 6613 (2022).

71. M. Liang, A. Mouraux, L. Hu, G. D. Iannetti, Primary sensory cortices contain distinguishable spatial patterns of activity for each sense. *Nat. Commun.* **4**, 1979 (2013).

72. Y. Gu, L. E. Sainburg, S. Kuang, F. Han, J. W. Williams, Y. Liu, N. Zhang, X. Zhang, D. A. Leopold, X. Liu, Brain activity fluctuations propagate as waves traversing the cortical hierarchy. *Cereb. Cortex* **31**, 3986–4005 (2021).

73. F. S. Bott, M. M. Nickel, V. D. Hohn, E. S. May, C. Gil Ávila, L. Tiemann, J. Gross, M. Ploner, Local brain oscillations and interregional connectivity differentially serve sensory and expectation effects on pain. *Sci. Adv.* **9**, eadd7572 (2023).

74. M. M. Nickel, L. Tiemann, V. D. Hohn, E. S. May, C. Gil Ávila, F. Eippert, M. Ploner, Temporal-spectral signaling of sensory information and expectations in the cerebral processing of pain. *Proc. Natl. Acad. Sci. U.S.A.* **119**, e2116616119 (2022).

75. J. Onysk, N. Gregory, M. Whitefield, M. Jain, G. Turner, B. Seymour, F. Mancini, Statistical learning shapes pain perception and prediction independently of external cues. *elife* **12**, RP90634 (2024).

76. M. Roy, D. Shohamy, N. Daw, M. Jepma, G. E. Wimmer, T. D. Wager, Representation of aversive prediction errors in the human periaqueductal gray. *Nat. Neurosci.* **17**, 1607–1612 (2014).

77. A. Strube, B. Horing, M. Rose, C. Büchel, Agency affects pain inference through prior shift as opposed to likelihood precision modulation in a Bayesian pain model. *Neuron* **111**, 1136–1151.e7 (2023).

78. J. Kim, A. Joshi, L. Frank, K. Ganguly, Cortical-hippocampal coupling during manifold exploration in motor cortex. *Nature* **613**, 103–110 (2023).

79. S. K. Wandelt, D. A. Bjånes, K. Pejsa, B. Lee, C. Liu, R. A. Andersen, Representation of internal speech by single neurons in human supramarginal gyrus. *Nat. Hum. Behav.* **8**, 1136–1149 (2024).

80. E. G. Duerden, M.-C. Albanese, Localization of pain-related brain activation: A meta-analysis of neuroimaging data. *Hum. Brain Mapp.* **34**, 109–149 (2013).

81. M. Čeko, P. A. Kragel, C.-W. Woo, M. López-Solà, T. D. Wager, Common and stimulus-type-specific brain representations of negative affect. *Nat. Neurosci.* **25**, 760–770 (2022).

82. L. Koban, M. Jepma, M. López-Solà, T. D. Wager, Different brain networks mediate the effects of social and conditioned expectations on pain. *Nat. Commun.* **10**, 4096 (2019).

83. M. O. Ernst, Learning to integrate arbitrary signals from vision and touch. *J. Vis.* **7**, 7.1-14 (2007).

84. C. R. Fetsch, A. H. Turner, G. C. DeAngelis, D. E. Angelaki, Dynamic reweighting of visual and vestibular cues during self-motion perception. *J. Neurosci.* **29**, 15601–15612 (2009).

85. N. W. Roach, J. Heron, P. V. McGraw, Resolving multisensory conflict: A strategy for balancing the costs and benefits of audio-visual integration. *Proc. Biol. Sci.* **273**, 2159–2168 (2006).

86. R. C. Coghill, *The Distributed Nociceptive System: A Framework for Understanding Pain*. Elsevier Ltd. [Preprint] (2020). https://doi.org/10.1016/j.tins.2020.07.004.

87. J.-J. Lee, S. Lee, D. H. Lee, C.-W. Woo, Functional brain reconfiguration during sustained pain. *eLife* **11**, e74463 (2022).

88. J. D. Semedo, A. Zandvakili, C. K. Machens, B. M. Yu, A. Kohn, Cortical areas interact through a communication subspace. *Neuron* **102**, 249–259.e4 (2019).

89. T. Zhang, J. S. Gao, T. Çukur, J. L. Gallant, Voxel-based state space modeling recovers task-related cognitive states in naturalistic fMRI experiments. *Front. Neurosci.* **14**, 565976 (2020).

90. Y. J. John, K. S. Sawyer, K. Srinivasan, E. J. Müller, B. R. Munn, J. M. Shine, It's about time: Linking dynamical systems with human neuroimaging to understand the brain. *Netw. Neurosci.* **6**, 960–979 (2022).

91. M. Venkatesh, J. Jaja, L. Pessoa, Brain dynamics and temporal trajectories during task and naturalistic processing. *Neuroimage* **186**, 410–423 (2019).

92. S. Gim, S.-J. Hong, E. A. Reynolds Losin, C.-W. Woo, Temporal dynamics of brain mediation in predictive cue-induced pain modulation. bioRxiv 576786 [Preprint] (2024). https://doi.org/10.1101/2024.01.23.576786.

93. M. Jepma, M. Jones, T. D. Wager, The dynamics of pain: Evidence for simultaneous site-specific habituation and site-nonspecific sensitization in thermal pain. *J. Pain* **15**, 734–746 (2014).

94. L. M. Bartoshuk, V. B. Duffy, B. G. Green, H. J. Hoffman, C.-W. Ko, L. A. Lucchina, L. E. Marks, D. J. Snyder, J. M. Weiffenbach, Valid across-group comparisons with labeled scales: The gLMS versus magnitude matching. *Physiol. Behav.* **82**, 109–114 (2004).

95. W. Yoshida, B. Seymour, M. Koltzenburg, R. J. Dolan, Uncertainty increases pain: Evidence for a novel mechanism of pain modulation involving the periaqueductal gray. *J. Neurosci.* **33**, 5638–5646 (2013).

96. L. Y. Atlas, N. Bolger, M. A. Lindquist, T. D. Wager, Brain mediators of predictive cue effects on perceived pain. *J. Neurosci.* **30**, 12964–12977 (2010).

97. R. H. R. Pruim, M. Mennes, D. van Rooij, A. Llera, J. K. Buitelaar, C. F. Beckmann, ICA-AROMA: A robust ICA-based strategy for removing motion artifacts from fMRI data. *Neuroimage* **112**, 267–277 (2015).

98. H. Singmann, D. Kellen, "An introduction to mixed models for experimental psychology" in *New Methods in Cognitive Psychology* (Routledge, 2019), pp. 4–31.

99. R. Vos de Wael, O. Benkarim, C. Paquola, S. Lariviere, J. Royer, S. Tavakol, T. Xu, S.-J. Hong, G. Langs, S. Valk, B. Misic, M. Milham, D. Margulies, J. Smallwood, B. C. Bernhardt, BrainSpace: A toolbox for the analysis of macroscale gradients in neuroimaging and connectomics datasets. *Commun. Biol.* **3**, 103 (2020).